Ion collection by a sphere in a flowing plasma: 3. Floating potential and drag force

2005 Plasma Phys. Control. Fusion 47 71

(http://iopscience.iop.org/0741-3335/47/1/005)

INSTITUTE OF PHYSICS PUBLISHING PLASMA PHYSICS AND CONTROLLED FUSION

Plasma Phys. Control. Fusion **47** (2005) 71–87 doi:10.1088/0741-3335/47/1/005

Ion collection by a sphere in a flowing plasma: 3. Floating potential and drag force

I H Hutchinson

Plasma Science and Fusion Center, Massachusetts Institute of Technology, Cambridge, MA, USA

Received 6 August 2004, in final form 9 September 2004
Published 9 December 2004
Online at stacks.iop.org/PPCF/47/71

Abstract

The interaction of an ion-collecting sphere at floating potential with a flowing collisionless plasma is investigated using the particle in cell code SCEPTIC. The dependence of the floating potential on the flow velocity for a conducting sphere is found to agree very well with the orbital motion limited approximation, which ignores the asymmetry in the plasma potential. But the charge, even on conducting spheres and at zero flow, is not well represented by using the standard expression for capacitance. Insulating spheres become asymmetrically charged because of ion collection asymmetry, and their total (negative) charge is considerably increased by flow. The collection flux asymmetry is documented for both conducting and insulating spheres and is not greatly different between them. The drag force upon the sphere is obtained from the code calculations. It shows reasonable agreement with appropriate analytic approximations. However, numerical discrepancies up to 20% are found, which are attributed to uncertainties in the analytical values.

(Some figures in this article are in colour only in the electronic version)

1. Introduction

In the first two papers of this series [1, 2] the 'Specialized Coordinate Electrostatic Particle and Thermals In Cell' (SCEPTIC) particle in cell code was described and calculations of the ion collection from a flowing collisionless plasma were made with a specified potential on the spherical collector. This paper addresses the situation that is more appropriate to an isolated spherical object, namely where the sum of ion and electron currents to the sphere is zero, and the probe adopts a potential, the floating potential, that self-consistently enforces this current balance. Code calculations are also given of the total force exerted on the sphere by the flowing plasma. This force is of crucial importance to the problem of dusty plasmas, and the present results are the first for a collisionless plasma to take account of the full self-consistent potential. They reveal discrepancies amounting to as large as 20% with the standard analytic expressions, in parameter regimes where the analytic approximations might have been expected to be more

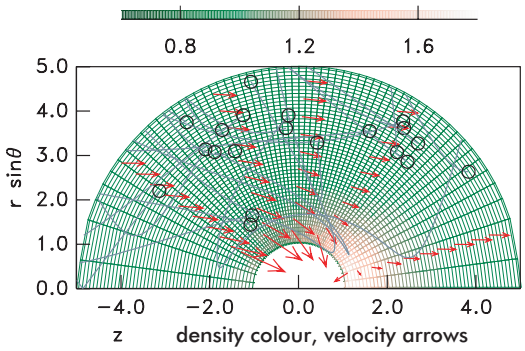

Figure 1. Computational grid of SCEPTIC. Colour contours indicate the ion density, normalized to the value at infinity. Density is enhanced immediately downstream from the probe. Arrows show the mean (fluid) velocity, normalized to $\sqrt{ZT_e/m_i}$. The external flow (left to right) for this case is unity. The tracks of 20 (out of about seven million) particle orbits are shown.

accurate. They also provide definitive values in regimes where no analytic approximation is justified.

Since SCEPTIC has been described before in detail [1, 2], only a summary is given here. It calculates the collisionless ion orbits in three dimensions and the self-consistent potential on a spherical mesh having rotational symmetry about the external plasma flow direction, using a Boltzmann factor for the electron density and solving the resulting Poisson equation. The ions are injected on an outer computational boundary in a manner that quite accurately represents a drifting Maxwellian distribution at infinity, and are perfectly absorbed by the spherical surface at the inner computational boundary. Figure 1 illustrates an example case. Most calculations reported here were made on a 100×100 $(r \times \theta)$ grid, with seven million particles. The potential is axisymmetric about the z-axis.

In the case with finite flow, a distinction arises between a conducting isolated sphere, which we here call 'floating', and a non-conducting, or 'insulating', sphere. The insulating sphere acquires a surface potential that varies with position on the surface so as to make the local current-density zero, whereas the floating sphere is an equipotential, whose value makes the total current zero.

Prior theories of the interaction of an absorbing sphere with a plasma have almost all used some form of spherically symmetric potential profile. It is, of course, standard practice to approximate the plasma-shielded potential of a charge as a vacuum $(1/r)$ form cut-off at a distance equal to the Debye-length, λ_D. When λ_D is much greater than the smallest relevant impact parameter (dictated, for a point charge, by 90° scattering or quantum-mechanical effects) the resulting Coulomb logarithm is insensitive to exact cut-off values. However, when dealing with a charged sphere of finite radius, r_p, the lower cut-off, which is at least $\geqslant r_p$, may not be much smaller than λ_D. Then a more careful calculation is necessary. The Debye–Hückel form of the potential ($\propto \exp(-r/\lambda_s)/r$) was used in some early numerical studies of momentum transfer [3–6] but is based on several approximations of questionable precision. It linearizes the equations, assuming the potential is much less than the electron temperature ($e\phi \ll T_e$), which is never valid close to a floating sphere; it ignores the absorption of charges, which causes the potential far from the sphere to have in reality a $\propto r^{-2}$ form [2, 7], rather than exponential; and it suffers from ambiguity about how to account for ion contributions to shielding; in other words, how is the shielding length, λ_s, related to λ_{De}? Daugherty *et al* [8] have addressed some of these questions in a study based on the kinetic theory formulation

of Bernstein and Rabinowitz [9] for isotropic mono-energetic ions, which can be solved as a differential equation, unlike the full Maxwellian distribution solved by Laframboise [10], which requires an integro-differential solution. They conclude that the Debye–Hückel form is a reasonable approximation only if $r_p \ll \lambda_s$, in which case the shielding length is smaller than λ_{De} by a factor $[2E_0/(T_e + 2E_0)]^{1/2}$, where E_0 is the ion energy. Ambiguity still remains as to how exactly to relate E_0 to a Maxwellian ion temperature. Kilgore *et al* [11] derived ion momentum scattering cross-sections based on the potential forms of Daugherty *et al*, finding little difference between results from the kinetic theory and the Debye–Hückel potential forms. Choi and Kushner [12] developed comparable results from a full-scale PIC simulation, including collisions and nonthermal electron effects, but ignoring ion drift. These agreed well with Kilgore *et al*'s. Khrapak *et al* [13] have compared the results of Kilgore and Hahn and developed convenient numerical fits to give the ion drag force (see later, equation (9)).

All these prior treatments effectively ignore the flow of the background ions, which will clearly affect the ion contribution to shielding, and they assume the plasma potential to be spherically symmetric. The present SCEPTIC calculations, in contrast, treat the ions fully self-consistently, assuming a drifting Maxwellian distribution at infinity, and make no assumptions about potential symmetry. They therefore provide a critical quantitative test of the errors introduced by the prior approximations.

2. Sphere potential and charge

The floating potential of a surface that has no charged particle emission is that potential at which the electron collection current-density,

$$\Gamma_e(\phi) = \Gamma_e(0) \exp\left(\frac{e\phi}{T_e}\right) = \frac{1}{4} n_{e\infty} \left(\frac{8T_e}{\pi m_e}\right)^{1/2} \exp\left(\frac{e\phi}{T_e}\right) \tag{1}$$

is equal to the ion collection current-density. The ion current-density is obtained in SCEPTIC by averaging the flux from typically 40 prior steps of the code. The resulting potential is used as the boundary condition in the potential solving step, thus producing in the steady state a self-consistent floating potential. For the insulating sphere, the local current-density is used to derive the local potential equal to $(T_e/e) \ln |Z\Gamma_i/\Gamma_e(0)|$. The statistics in this case can become poor for surfaces with low ion currents. For the floating conducting sphere, the total current over the entire surface is zeroed by using the surface average of the ion flux in this formula.

Stationary plasma probe theory gives the value of the ion flux, which we express in the form

$$Z\Gamma_i = f n_{e\infty} \sqrt{\frac{ZT_e}{m_i}}, \tag{2}$$

where the factor f ranges from approximately 0.5 for small Debye-length to the orbital motion limited (OML) value $(Ze\phi/T_i + 1)\sqrt{T_i/ZT_e}/\sqrt{2\pi}$, for large Debye-length. (The OML approximation [14], or see, e.g. [15] for an introduction, assumes that no intermediate effective potential barrier repels the ions. If no barrier exists, then the collection can be determined by energy and angular momentum conservation applied at the collector). In the case of a Maxwellian ion distribution drifting with velocity $v_f = U\sqrt{2T_i/m_i}$, and a negatively charged sphere of potential $\phi = -\chi T_i/Z$, an OML value for average flux density can be obtained if

one approximates the potential as spherically symmetric, yielding [2, 16] [1]

$$f = \sqrt{\frac{2T_\mathrm{i}}{ZT_\mathrm{e}}}\frac{U}{4}\left\{\left(1+\frac{1}{2U^2}+\frac{\chi}{U^2}\right)\mathrm{erf}(U)+\frac{1}{U\sqrt{\pi}}\exp(-U^2)\right\}. \tag{3}$$

But of course once the problem's symmetry is broken by flow, a symmetric potential is an approximation of *a priori* unknown accuracy.

The floating potential is then the solution of

$$\phi_\mathrm{f} = \frac{T_\mathrm{e}}{e}\left(\frac{1}{2}\ln\left|\frac{2\pi Zm_\mathrm{e}}{m_\mathrm{i}}\right|+\ln|f|\right). \tag{4}$$

The first term in the bracket is -2.84 for hydrogen and -4.68 for singly-charged argon, leading to typical floating potentials of roughly 2–5 times T_e/e. This is sufficiently negative to justify the use of the Boltzmann factor for electrons, if the distant electron distribution function is Maxwellian. Incidentally, when f is a function of ϕ_f, through χ, then equation (4) is an excellent form for solving the transcendental equation in a few iterations.

From the viewpoint of the SCEPTIC calculation, or indeed any calculation of the plasma behaviour, all that is essential is the sphere potential. However, knowledge of the total charge on the sphere is often desired. This may be obtained by applying Gauss's Law to the sphere surface. However, the potential derivative there includes the effect of plasma shielding. Based on the standard Debye shielding form, $\phi \propto \exp(r/\lambda_\mathrm{s})/r$, we have $E_r = \phi(1/r + 1/\lambda_\mathrm{s})$, showing that when the Debye-length becomes short, the charge, $4\pi\epsilon_0 r^2 E_r$, becomes large, and the capacitance of the sphere becomes larger by a factor of approximately $1+r/\lambda_\mathrm{s}$ than the vacuum value, $4\pi\epsilon_0 r$. The capacitance also becomes troublesome to calculate accurately, since the condition justifying the Debye shielding approximation, namely $|\phi e/T_\mathrm{e}| \ll 1$, is not satisfied for a floating sphere, and so accurate values require a self-consistent nonlinear calculation. All these theoretical difficulties are magnified when the plasma flow velocity is included and breaks the spherical symmetry. The SCEPTIC calculation takes all the complicating factors consistently into account and so can evaluate how important they are quantitatively.

2.1. Conducting sphere floating potential

In figure 2 are shown examples of the floating potential for an equipotential sphere in a hydrogenic plasma ($m_\mathrm{i} = 1837m_\mathrm{e}$, $Z = 1$) compared with the values derived from the OML approximation, equations (3) and (4). The agreement is remarkably good, within the code uncertainty of perhaps 2% judged by the scatter, for all but a couple of points near $v_\mathrm{f} = 1$, except that at low velocity and temperature, when $\lambda_\mathrm{De} \sim 1$, the potential is dropping, indicating a gradual breakdown of the OML assumptions there. (The 2% uncertainty in ϕ_f corresponds to an uncertainty of about 4% in flux, which is larger than in earlier SCEPTIC calculations in part because of using a larger computational domain radius for these long Debye-length cases.)

The agreement shows that the effects of asymmetry in the potential are virtually negligible with respect to the total ion flux. In itself this is a new and valuable result. Prior multidimensional PIC results [17] treating the electrons, as well as the ions, via particle dynamics (unlike SCEPTIC) had uncertainties too large to validate the OML model even with an artificially low mass ratio ($m_\mathrm{i} = 100m_\mathrm{e}$).

To illustrate the relatively small potential asymmetry, which is presumably the reason for the success of the OML result, figure 3 shows two-dimensional contour plots of the potential and density for a low-ion-temperature case. This case is comparatively strongly

[1] When evaluation of the error functions is inconvenient, equation (3) may be approximated to an accuracy better than 2% as $f \approx (U^2+4/\pi)^{1/2}[1+\chi/(U^{2\kappa}+1)^{1/\kappa}]/4$ with $\kappa = 1.17$.

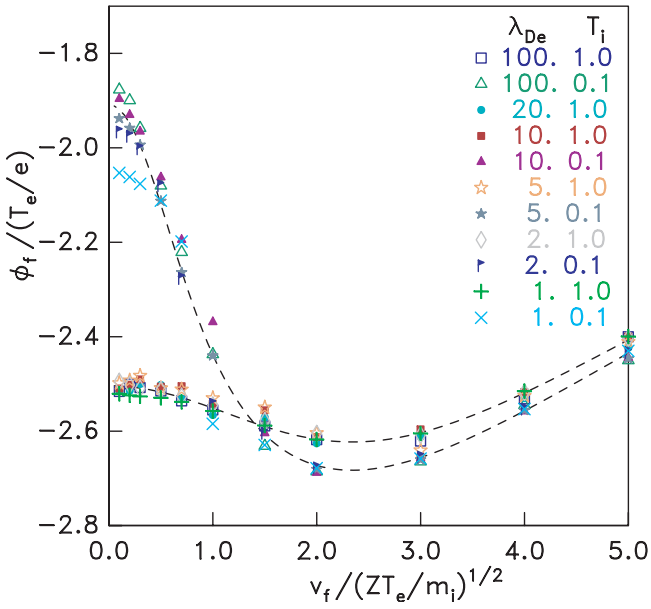

Figure 2. Floating potential calculated by SCEPTIC as a function of normalized drift velocity, for a range of λ_{De} measured in units of the sphere radius, and for $T_i = 1$ and 0.1 times ZT_e. The dashed line shows the OML theory.

asymmetric. The density asymmetry consists of a substantially enhanced wake region, caused by ion focusing, accompanied by a trailing cone of mild (∼10%) rarefaction. Still the potential asymmetry is modest. And in the upstream region, where the strongest effects on collection may be expected, it is visibly very small, even with the logarithmic contour spacing used here.

There is, even for a low temperature, no evidence whatever in the SCEPTIC results of a tendency for the floating potential to tend to zero as the ratio of the Debye-length to the probe size becomes large. Such a counter-intuitive limit has been proposed [18] on the basis of the ABR treatment [19], which accounts only for radial ion motion. This present work, of course, completely excludes collisions. Consequently angular momentum, whose conservation is ignored in the ABR approach, is not dissipated here by collisions. Nevertheless, this work shows that even when the angular momentum conservation is imperfect because of small potential asymmetries, the effect on the floating potential is negligible. This suggests that the ABR approximation in the long-Debye-length limit is hardly credible. Its ignoring collisional effects on radial motion while supposing the angular momentum to be totally dissipated collisionally would call for extreme sensitivity of the floating potential to angular momentum conservation violation. The present results show such sensitivity to be absent. A more recent radial motion theory [20] shows that including collisional drag in the radial equation enhances the floating potential relative to the collisionless ABR treatment. But a proper accounting for collisions really requires the inclusion of collisions in a multidimensional calculation, such as the work of Choi and Kushner [12], which, like the present results, shows only weak variation of the floating potential with particle size, when $\lambda_{De} \gg$ sphere radius.

2.2. Charge and capacitance

The charge on the sphere when it is floating is of course mostly a reflection of its floating potential and capacitance. In figure 4 is shown the total sphere charge determined from SCEPTIC for

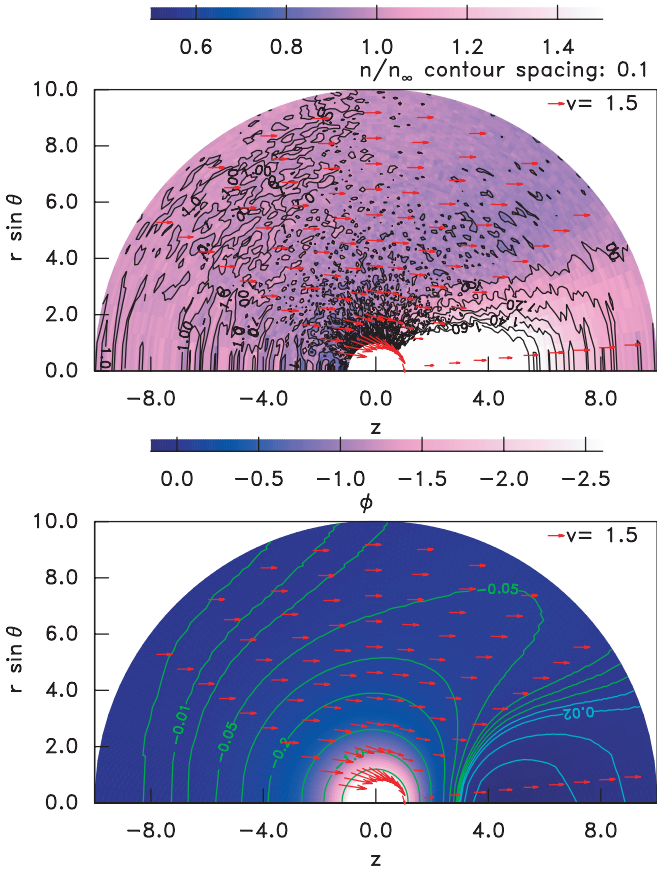

Figure 3. Contour plots of density (upper) and potential (lower) for a floating sphere when $T_i = 0.1T_e$, $v_f = 1.5\sqrt{ZT_e/m_i}$, $\lambda_{De} = 2r_p$, $m_i = 1837m_e$. The arrows show the mean ion velocity. The potential contours are logarithmically spaced.

a range of Debye-lengths. The charge, Q, is expressed in normalized units as $Q/(\epsilon_0 r_p T_e/e)$, where r_p is the sphere radius. The floating equipotential sphere shows little variation in the total charge with flow velocity. In contrast there is a substantial increase of total (negative) charge with flow velocity for an insulating probe. This effect is caused by the strong negative potential that develops on the downstream side of the sphere for supersonic flow, because the flux on that side is much smaller. This effect also causes greater statistical uncertainty in the charge at the highest flows, as can be seen particularly in the $\lambda_{De} = 10$ case in figure 4.

This figure also shows the charge that would be predicted using the OML potential (which figure 2 shows to be quite accurate) and for capacitance the expression appropriate to the linearized plasma shielding approximation $C = 4\pi\epsilon_0 r_p(1 + 1/\lambda_{De})$ (see, e.g. [16]). This formula reproduces SCEPTIC's floating values very well for $\lambda_{De} = 100$ and 10, but not nearly so well for $\lambda_{De} = 2$ and 1. If one uses a shorter value for the screening length, λ_s, accounting for ion contribution to shielding, in the capacitance formula, the discrepancy is even larger. This discrepancy illustrates the inadequacy of the linearized approximation to the capacitance. Although flow makes this inadequacy somewhat worse (when one uses λ_{De} but not if one uses λ_s), the problem is present even at zero velocity. SCEPTIC of course calculates the full self-consistent potential and charge, and hence capacitance.

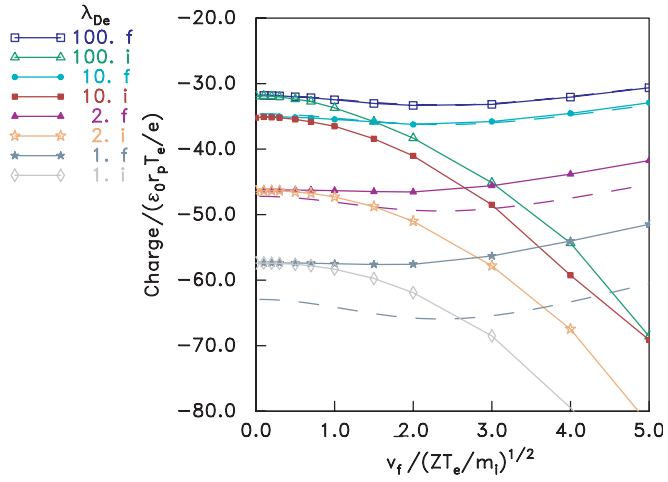

Figure 4. Charge as a function of drift velocity for an isolated sphere in a hydrogenic plasma ($m_i = 1837m_e$, $T_i = ZT_e$). A range of Debye-lengths (λ_{De}) are plotted, and both floating (f) and insulating (i) spheres. Dashed lines show the linearized-capacitance analytic approximation.

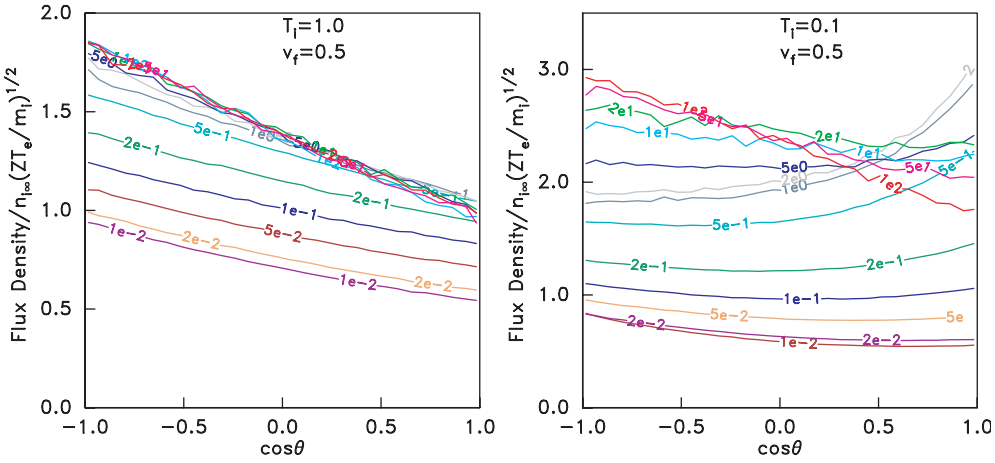

Figure 5. Flux density as a function of angle for a floating sphere for various values of λ_{De} normalized to the sphere radius (labels embedded in lines), fixed flow velocity, $m_i/m_e = 1837$ (hydrogen).

2.3. Flux asymmetry

As has been discussed in detail in [2], the angular distribution of ion flux to the sphere varies strongly with Debye-length. In figure 5 is shown the angular distribution for a fixed velocity $v_f = 0.5$ (in normalized units of $\sqrt{ZT_e/m_i}$) for a wide range of λ_{De} (normalized to the sphere radius), when the sphere is floating. The low ion temperature case ($T_i = 0.1$ in units of ZT_e) shows the reversal of asymmetry previously reported [2], but in this case specifically for a floating potential.

For an insulating sphere the flux distributions are qualitatively very similar. In figure 6 are shown the data in the form of the sphere potential, which contains the same information as the flux, since for an insulating sphere they are related via equation (4).

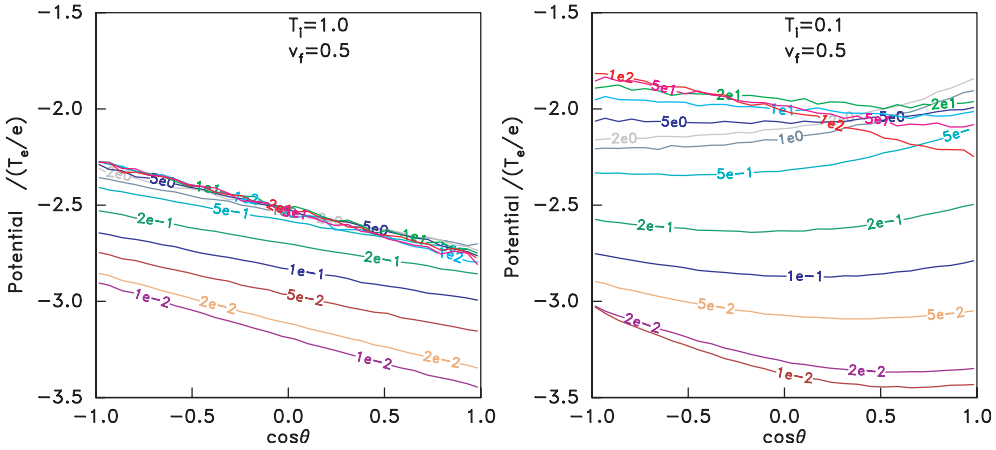

Figure 6. Surface potential as a function of angle for an insulating sphere for various values of λ_{De} normalized to the sphere radius, fixed flow velocity, $m_i/m_e = 1837$ (hydrogen).

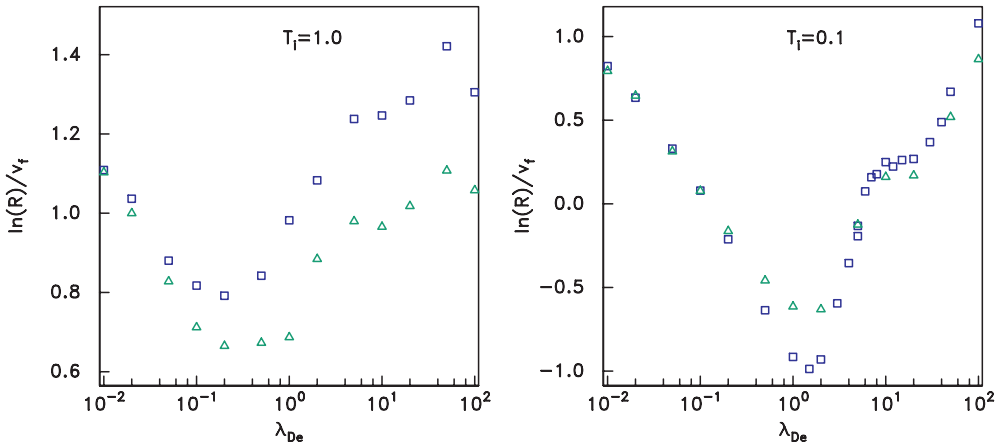

Figure 7. Asymmetry factor, $\ln(R)/v_f$, as a function of Debye-length normalized to sphere radius. □, floating sphere; △, insulating sphere.

The flux asymmetry is conveniently summarized by the ratio of the upstream (axial) flux density to the downstream flux density, R. Then for a subsonic flow the single calibration factor $K = \ln|R|/v_f$ represents the asymmetry. In figure 7 are shown the dependences on the Debye-length of the calibration factor, K, for both floating and insulating spheres. Although the values obtained are for a specific flow velocity, $v_f = 0.5$, they are approximately independent of v_f when the flow is subsonic. The numerical values for floating and insulating spheres are rather similar, showing that the potential asymmetries on the sphere surface in the insulating case, though substantial, do not affect the collection flux very much.

The region around $\lambda_{De} \sim 10$ has been explored in more detail in figure 7 to show the fine-scale structure there. In figure 8, the upstream and downstream flux densities are plotted separately. These data show that the structure there is in fact quite noticeable, almost a cusp on this log plot, and arises from the downstream flux density variation. We can also observe the effective noise level of these fluxes to be roughly 3% in this region. This enhanced level

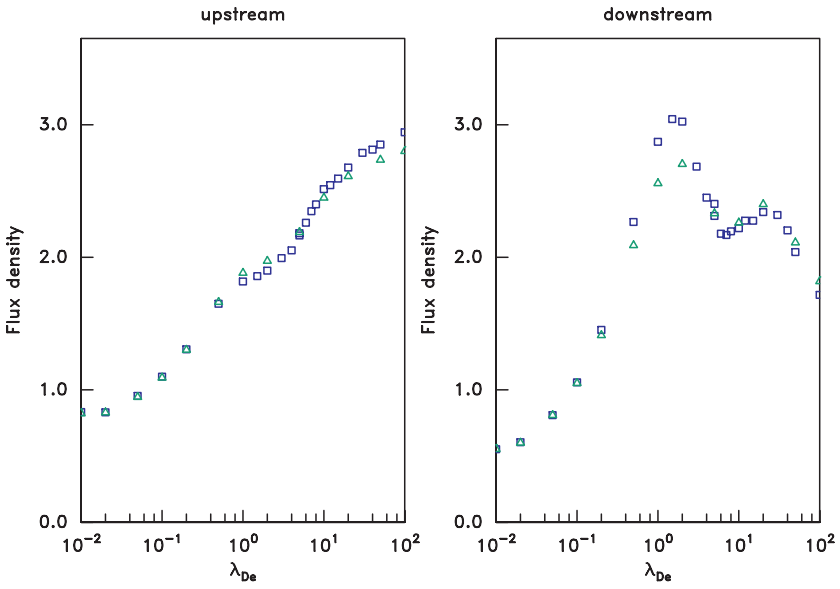

Figure 8. Flux density (in units of $n_{i\infty}\sqrt{ZT_e/m_i}$) on the upstream and downstream axial positions as a function of Debye-length (in units of r_p), for drift velocity $v_f = 0.5$ (times $\sqrt{ZT_e/m_i}$). □, floating sphere; △, insulating sphere.

(relative to the short Debye-length cases) again arises because a larger domain size of 15 times the probe radius has been adopted to avoid boundary effects on the flux.

3. Drag force

A problem of particular importance for an isolated sphere in a flowing plasma is the question of what drag force it experiences. A sphere of infinitesimal size would be governed by the standard calculation of the drag on a point charge in a plasma. However, a finite sphere size introduces a number of complications. First the charge on the sphere must be determined self-consistently, and of course is generally macroscopic, many times the elementary charge. Second, the sphere directly absorbs some of the plasma particles, thus directly acquiring their momentum and making it improper to continue an impact parameter integration of a Coulomb orbit expression to lower values than the value at which absorption occurs. Third, both these effects reduce the effective value of the Coulomb logarithm, and thereby often undermine the validity of the approximations made in the standard point-charge treatment. For example, it is not unusual for dust particles in plasmas to have a radius that is a significant fraction of the Debye-length.

3.1. Coulomb collision analytic treatment

Most discussions of drag on grains in plasmas use some variation of the standard point-charge treatment, which has its origin in Chandrasekhar's [21] calculations of the drag on a moving star, interacting with its neighbours via an inverse-square force. This calculation considers the momentum transfer from hyperbolic orbits of the neighbours relative to the sphere, leading, for field particles of velocity $\boldsymbol{v}_1$, to an integration over impact parameters b of the $\hat{\boldsymbol{x}}$-direction

momentum transfer in the form

$$F_{\rm o} = \int\!\!\int_0^{b_{\max}} 2m_r v_r \boldsymbol{v}_r \cdot \hat{\boldsymbol{x}} f(\boldsymbol{v}_1) \, \frac{1}{b^2/b_{90}^2 + 1} \, 2\pi b \, {\rm d}b \, {\rm d}^3 v_1, \tag{5}$$

where $m_r \equiv m_1 m_2/(m_1+m_2)$ is the reduced mass, $\boldsymbol{v}_r = \boldsymbol{v}_1 - \boldsymbol{v}_2$ is the relative velocity, $f(\boldsymbol{v}_1)$ is the velocity distribution function and $b_{90} = q_1 q_2/4\pi\epsilon_0 m_r v_r^2$ is the impact parameter for 90° scattering in the centre of mass frame, which has here been written for the electrostatic force between charges q_1 and q_2. The upper limit of the otherwise divergent b-integral must be taken as corresponding to the place where the two-body interaction can no longer be taken as inverse square. Chandrasekhar thought that this distance was the mean interstellar distance, but it was later demonstrated [22] that it is a shielding length, $\lambda_{\rm s}$, approximately equal to the Debye-length. Although it is possible to treat classical near collisions exactly, most elementary derivations use a small-scattering-angle approximation ($b \gg b_{90}$) and then obtain the integral of $1/b$, to which has to be applied a minimum impact parameter cut-off at b_{90}. If the resulting term $\ln|b_{\max}/b_{\min}| \equiv \ln\Lambda$, from the b-integration, is taken as approximately independent of velocity, the velocity integrals for a Maxwellian distribution can be performed to obtain

$$F_{\rm o} = 8\pi \left(\frac{q_1 q_2}{4\pi\epsilon_0}\right)^2 \frac{n_1}{m_r v_n^2} \ln\Lambda \; G(u) \; , \tag{6}$$

where $v_n = \sqrt{2T_1/m_1}$ is the thermal velocity of the field particles (1), $u = v_2/v_n$ denotes the normalized drift velocity of the test particle (2), the sphere in our case, relative to the mean velocity of the field particles (which are assumed to have a Maxwellian distribution), and

$$G(u) \equiv \frac{{\rm erf}(u) - 2u{\rm e}^{-u^2}/\sqrt{\pi}}{2u^2}, \tag{7}$$

which is frequently used in its small argument limit, $G(u) \approx 2u/(3\sqrt{\pi})$ for $u \ll 1$. The standard [23–25] extension of this treatment to a finite sphere consists of taking the lower limit of the impact parameter integration at the critical impact parameter below which the particle collides with the sphere, $b_{\rm c}$. When this is done, the drag force due to non-collected particles differs from the point-charge calculation (equation (6)), only in the substitution

$$\ln\Lambda \approx \ln\frac{\lambda_{\rm s}}{b_{90}} \to \frac{1}{2}\ln\left|\frac{b_{90}^2 + \lambda_{\rm s}^2}{b_{90}^2 + b_{\rm c}^2}\right|. \tag{8}$$

In all such calculations the presumption is made that $\lambda_{\rm s}/b_{90}$ is large, the Coulomb logarithm is therefore a very weak function of its argument and that therefore it is adequate for purposes of integration over a distribution function to substitute into this expression a 'typical' velocity, which is usually [22,26,27] taken as $v_{\rm t} = (3T/m)^{1/2}$, although some authors [11,28] effectively use $v_{\rm t} = (2T/m)^{1/2}$. For a Maxwellian drifting with velocity $v_{\rm f}$, a consistent extension to the first option is to take $v_{\rm t} = (v_{\rm f}^2 + 3T/m)^{1/2}$, which is adopted for comparisons here. The shielding length is taken as the combination of electron and ion Debye-lengths $1/\lambda_{\rm s}^2 = 1/\lambda_{\rm De}^2 + 1/\lambda_{\rm Di}^2$ using the above flow-corrected $v_{\rm t}$ for ions, although substantial ambiguity exists in this respect.

This treatment clearly is quantitatively unreliable when $\lambda_{\rm s}$ is no longer much greater than $b_{\rm c}$ or b_{90}. In such situations, a substantial contribution to the drag comes from orbits in regions where the field is partly shielded. Therefore the simple cut-off is no longer appropriate. Detailed calculations of the drag force coefficients for an assumed Debye–Hückel shielding potential of a point charge when $\lambda_{\rm s} \sim b_{90}$ were done long ago [3–5]. Recently, Khrapak *et al* [13] have shown that a reasonable numerical fit to those collision cross-sections [6] is obtained by using for the upper impact parameter cut-off, the orbit whose closest approach to

the charge is equal to the shielding length. This ansatz gives the same result as above, except that the Coulomb logarithm takes the form

$$\ln \Lambda \rightarrow \ln \left[\frac{b_{90} + \lambda_s}{b_{90} + b_c} \right], \tag{9}$$

where b_{90} here must be evaluated using $v_t = (v_f^2 + 2T/m)^{1/2}$. This $\ln \Lambda$ expression is not validated for non-zero b_c and actually gives scattering cross-sections when $b_c = 0$ that exceed the point-charge numerical results of Hahn by ∼7% over the relevant velocity range, despite the nominal identity of their potentials. Negative values for the logarithm when $\lambda_s < b_c$ are of course unphysical.

An important ambiguity remains in equation (6) for finite radius particles, regardless of which $\ln |\Lambda|$ expression is used. The question is what to use for the grain charge, q_2. Of course, the collisional drag is determined by the *potential* surrounding the charge, not the charge *per se*. If the potential has a Debye–Hückel form, $\phi = (q_{\rm eff}/4\pi\epsilon_0) \exp(-r/\lambda_s)/r$, then the effective point charge is related to the sphere potential, ϕ_p, via $q_{\rm eff} = 4\pi\epsilon_0\phi_p \exp(r_p/\lambda_s)r_p$, which is approximately the same as the actual charge, $q_p = -4\pi\epsilon_0 r_p^2\, {\rm d}\phi/{\rm d}r = q_{\rm eff}(\exp(-r_p/\lambda_s)/r_p)(1/\lambda_s + 1/r_p)$. However, in the important region where the orbit integration must be performed, the expression $\phi_p r_p/r$ is a better $1/r$–approximation to the potential than $q_{\rm eff}/4\pi\epsilon_0 r$. What is more, to obtain the correct OML collection impact parameter, b_c, a form that yields the correct potential at the sphere *must* be used. Therefore it appears more appropriate to use a value $q_2 = \phi_p 4\pi\epsilon_0 r_p$ in equation (6), and that choice is adopted here. (In a preliminary presentation of some of the present results [29], (and in figure 10 for comparison) the value $q_2 = q_{\rm eff}$ was adopted, and gives analytic drag force values that are about 20% higher at $\lambda_{De} = 10$. This is an indication of the approximate degree of uncertainty in the analytic estimates.)

To the expression (6) for the orbital drag force, F_o, must be added the momentum transfer rate due to direct ion collection, which we will denote F_c. This is sometimes taken as given by the OML ion collection rate times the average momentum [24, 25], which is an approximation that is exact only in the limit of negligible ion temperature. It is also incorrectly sometimes taken as equal to the momentum flux from a shifted Maxwellian neglecting the electric field [27, 30, 31]. The most consistent value to take is the OML momentum flux rate integrated over a shifted Maxwellian, which can be written

$$F_c = n_1 r_p^2 m_1 v_n^2 \frac{\sqrt{\pi}}{2} \left\{ u(2u^2 + 1 + 2\chi){\rm e}^{-u^2} + \left[4u^4 + 4u^2 - 1 - 2(1 - 2u^2)\chi\right] \frac{\sqrt{\pi}}{2} {\rm erf}(u) \right\} \times \{u^2\}^{-1}, \tag{10}$$

where $\chi \equiv -q_1\phi_p/T_1$ is the normalized sphere potential and r_p its radius. (The derivation of this formula, which is cited in [32], is elementary under the OML assumptions of spherical potential symmetry and absence of effective potential barriers, albeit involving fairly heavy algebra.)

There are several other forces on grains, arising from additional physical effects [25], that may need to be accounted for in practical situations, but we concern ourselves here with this idealized case, where only the plasma force due to flow, $F_o + F_c$, is considered.

3.2. Code evaluation of force

The SCEPTIC code can directly evaluate the drag force on the sphere. This evaluation is not trivial and is carried out in terms rather different from the Coulomb collision treatment.

Consider some surface S surrounding the sphere. The total momentum flux across that surface is responsible for the drag force on the sphere. (We here assume that it is reasonable to

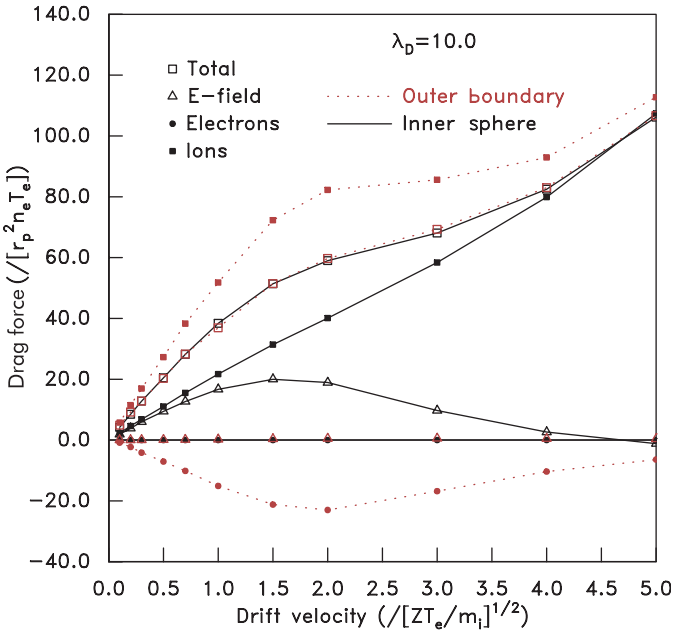

Figure 9. Example of SCEPTIC calculations for $\lambda_{De} = 10$, on a computational domain of radius 20 times the probe radius, with $T_i = ZT_e$. The contributions to the drag force at the inner and outer surfaces are different but add up to a consistent total.

take the sphere to be in steady, non-decelerating motion through the plasma either because it has sufficient total momentum or because it is acted on by other forces, which are not discussed.) The momentum flux consists of three components: (1) ion momentum flux; (2) electric field forces; (3) electron pressure. The ion momentum flux is obvious, and in the code is evaluated by summing the momentum of all ions crossing the surface. The electric field forces are expressed in terms of the Maxwell stress tensor,

$$\boldsymbol{F}_{\mathrm{E}} = \int_S \epsilon_{\mathrm{o}} \left(\frac{1}{2} E^2 1 - \boldsymbol{EE} \right) \mathbf{d}\boldsymbol{S}, \tag{11}$$

which gives the net electric force on all particles inside the surface. This also can be evaluated in the code. The stress tensor is derived from finite differences of the potential, known on the mesh. It is integrated over a spherical surface.

The electron pressure is also significant. Even though electrons do not possess significant drift momentum, because their mass is small, they respond to the local electric field, and in the model that SCEPTIC treats, their density is determined by the potential through the Boltzmann factor, while their temperature is uniform. Since electron pressure is comparable with ion pressure, asymmetries in electron pressure, arising from electron density asymmetries, are not negligible. The force is evaluated by an appropriate integral of the electron pressure over a spherical surface.

Note that these three contributions can be integrated over any surface surrounding the sphere. In a steady state, any such integration should give the same total momentum flux. In the SCEPTIC code, the two natural special surfaces to consider are the probe surface and the outer boundary of the simulation region. Figure 9 shows an example of the various contributions. Their share of the total is different at the two surfaces.

A good test of the accuracy and convergence of the code is whether the forces derived from these two different spheres of integration are the same. If the code is not converged, there are time derivatives of the total plasma momentum in the region between the two surfaces, and thus their momentum fluxes do not agree. More technically, if there are inaccuracies in the evaluation of any of the terms of the momentum flux, then discrepancies will arise. These latter discrepancies prove to be quite troublesome for the insulating probe cases. In such cases, the integration of the Maxwell stress tensor, which involves some delicate cancellations, quite often shows the effects of finite difference approximations inaccurately representing those cancellations, and the results being obviously unphysical. No such problematic cases are presented here.

At the inner boundary (sphere surface) the electron pressure contribution is negligible (exactly zero in this equipotential sphere case) and the ion collection momentum flux contribution increases monotonically with drift velocity. The electric field contribution, which corresponds to the drag from ions that miss the probe, shows a maximum at approximately the sound speed, falling off above it. This behaviour arises in the theoretical drag calculation from the velocity dependence of the collision cross-section, although here it simply emerges from the code result. At the outer edge of the computational domain, the electron pressure asymmetry contributes a substantial negative force, while the electric field force is negligible. The total is equal to that obtained from the sphere surface integration within about 3%, which may be taken as the uncertainty in the result.

For $\lambda_{De} \gtrsim 10$, the electron pressure force remains non-negligible at the outer boundary ($r = r_{max}$) even for the largest computational domains explored, when using the standard boundary conditions on the potential (described in detail in [2]). This effect is caused by an extended wake of enhanced ion density, which is why the pressure force component is negative (accelerating). Since this raises a question as to whether SCEPTIC is being biased by the boundary-condition, runs have also been performed using the alternative of setting $\phi = 0$ on the outer boundary, which forces the electron pressure to zero but, more important, strictly ensures that no drag arises from particles outside the computational domain. It is found that the *total* drag force is negligibly affected (<2%) for $r_{max} \gtrsim 2\lambda_{De}$, even though the balance of the force components in the outer region is changed. With $T_i = T_e$, for the more extreme case $r_{max} = \lambda_{De} = 10$, the total force is reduced by 10% using the $\phi = 0$ condition. Domain size explorations from $r_{max} = 40$ downwards, with standard boundary condition, show <2% variation until at $r_{max} = 10$ a force *increase* of 3% occurs. In short, drag-force errors arising from a finite domain size are negligible for $r_{max} \gtrsim 2\lambda_{De}$.

It might be thought that there is a direct equivalence of the decomposition into ion momentum and electric field at the sphere surface with the collection and orbit force components, F_c and F_o, of the theoretical description. However, figure 10 shows this is not accurate. Here we see that F_c is somewhat smaller than the ion momentum flux, and in compensation F_o is rather larger than the electric field component. (Equation (9), for $\ln \Lambda$ is used here.) The way this difference arises, which is qualitatively similar for a range of parameters, is that ions are accelerated in the potential well and arrive at the sphere with substantial momentum in addition to their initial momentum at a far distance. Since the collection flux of the ions is asymmetric, there is an asymmetry in the ion momentum collection that is not equal to the input ion momentum of the collected ions. In other words, the collected ions can exchange momentum with the electric field before being collected; and they do.

In figures 11 and 12 is shown a systematic scan of the Debye-length for ion temperatures of 1 and 0.1 (times ZT_e). The code results are compared with the theoretical drag, $F_o + F_c$, predicted by equations (6) and (10) with the alternative standard (equation (8)) and Khrapak (equation (9)) forms for $\ln \Lambda$. The value of $\ln \Lambda$, and hence F_o, is set to zero if those forms

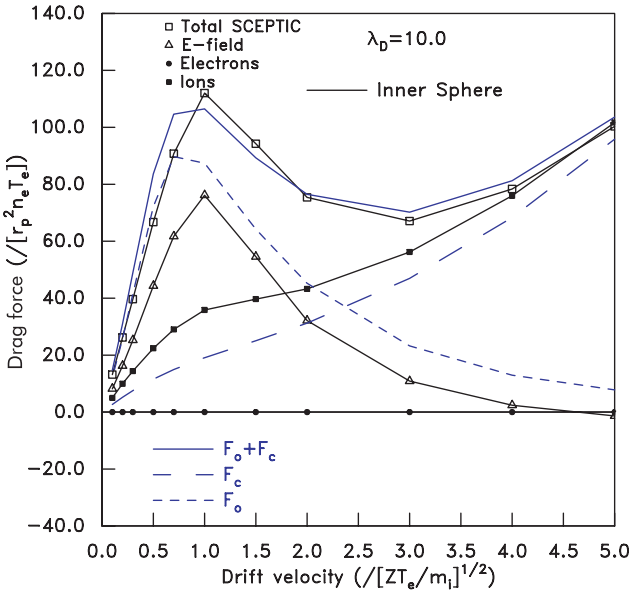

Figure 10. SCEPTIC calculations for $\lambda_{De} = 10$, on a computational domain of radius 20 times the probe radius, with $T_i = 0.1ZT_e$. The contributions to the drag force at the inner surface do not correspond exactly to the theoretical orbit and collection components (- - - -).

yield a negative $\ln\Lambda$. The dashed line shows the collection force, F_c, from equation (10). These results are for floating spheres, whose potential (at $r = 1$) for the analytic model is taken equal to whatever SCEPTIC determines. (Taking the model charge within $r = 1$ equal to the SCEPTIC-determined charge gives very similar results.)

The agreement is fairly satisfactory. The Khrapak form remains viable to a somewhat lower Debye-length than the standard form (all relative to sphere radius). But for the $T_i = 1$ cases there is little difference between the two analytic values for cases where F_o is significant.

Several additional verifications of SCEPTIC's results were undertaken. First, runs were performed with the angular acceleration turned off. This amounts to forcing perfect angular-momentum conservation, an assumption of the analytic theories. The sphere-surface force evaluation is still correct. Second, a potential independent of angle, whose radial dependence is equal to the angle-average of a full SCEPTIC run, was used. In this case, the outer domain boundary ion force is correct. Third, a run using the (angle-independent) Debye–Hückel potential approximation was performed. And finally, calculations were performed for the symmetric potential cases that used a totally independent angular integration method for obtaining the ion orbit and scattering angle. None of these results differed from the initial SCEPTIC results by more than about 3%. These tests therefore confirm SCEPTIC's accuracy and show that the discrepancies with the analytic results are not explained by potential asymmetries.

Therefore I attribute the discrepancy between SCEPTIC and the analytic formulae to the approximations in the analytic theories, but not to the assumption of spherical potential symmetry, or potential profile shape.

4. Conclusions

The computational results presented here are the first to take account of the full, nonlinear, asymmetric, self-consistent problem of collisionless flowing plasma interacting with floating

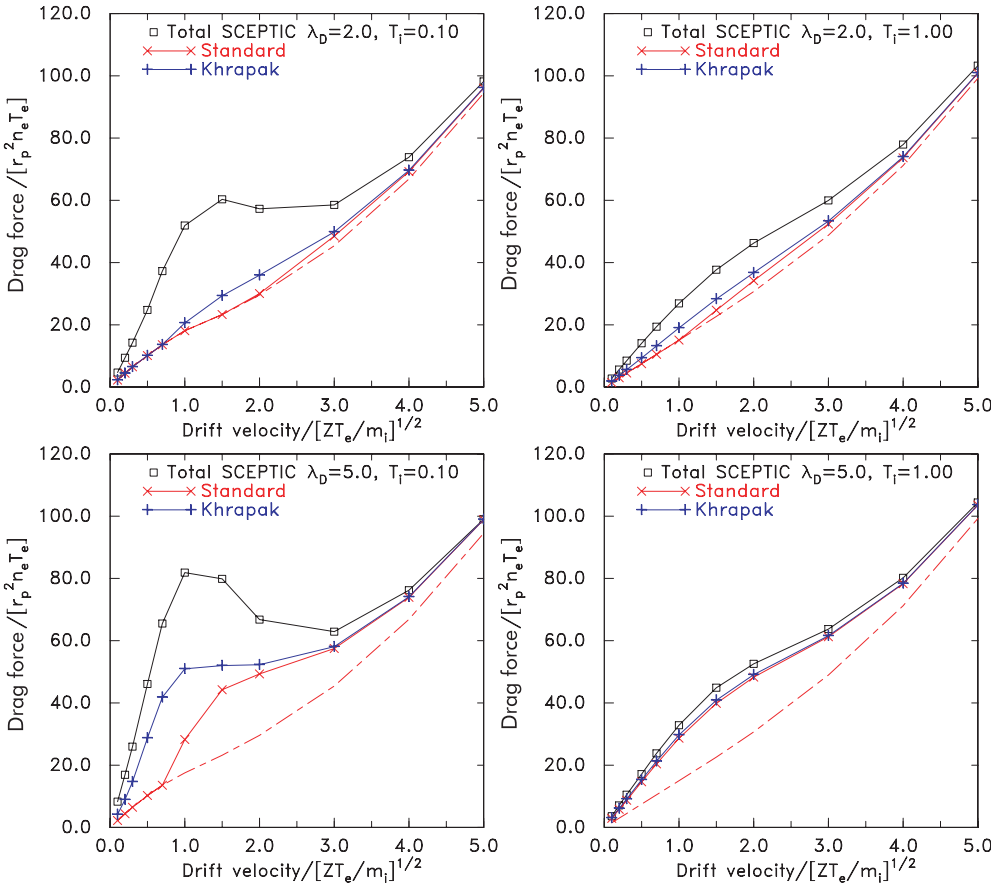

Figure 11. SCEPTIC calculations for $\lambda_{De} = 2$ and 5, on a computational domain of radius 10 and 20, respectively, times the probe radius, with $T_i = 0.1$ and 1.0 ZT_e.

or insulating spheres, at an accuracy that is sufficient for critical comparisons with approximate analytic theory. The results show that the asymmetry in the plasma potential is rather small for most situations and does not have a strong effect on the results. Consequently, the OML approximation, when it is justified by a large value of λ_{De}/r_p, provides a reliable measure of the total ion flux to a floating sphere, and hence its potential. Of course, the OML expression for a drifting ion distribution must be used. The charge on the sphere, however, is not well represented by typical analytic approximations to the capacitance, except when it is close to the vacuum value, because of the plasma nonlinearity. In other words, the approximation $e\phi/T_e \ll 1$, which justifies the Debye–Hückel potential form is, invalid close to the surface. The asymmetry in ion flux to the sphere surface is documented here for a wide range of Debye-lengths. When the flow is subsonic, the asymmetry proves not to be greatly different for floating and insulating spheres. However, for the insulating case, the potential is greatly depressed on the downstream side at high flow-velocities, which substantially increases the negative charge on the sphere.

The drag force, which is critical for many dusty plasma situations, has been directly calculated from the simulations. The effects of both direct particle collection flux and deflected ion orbits in the shielded sphere potential are fully accounted for. Reasonable agreement is

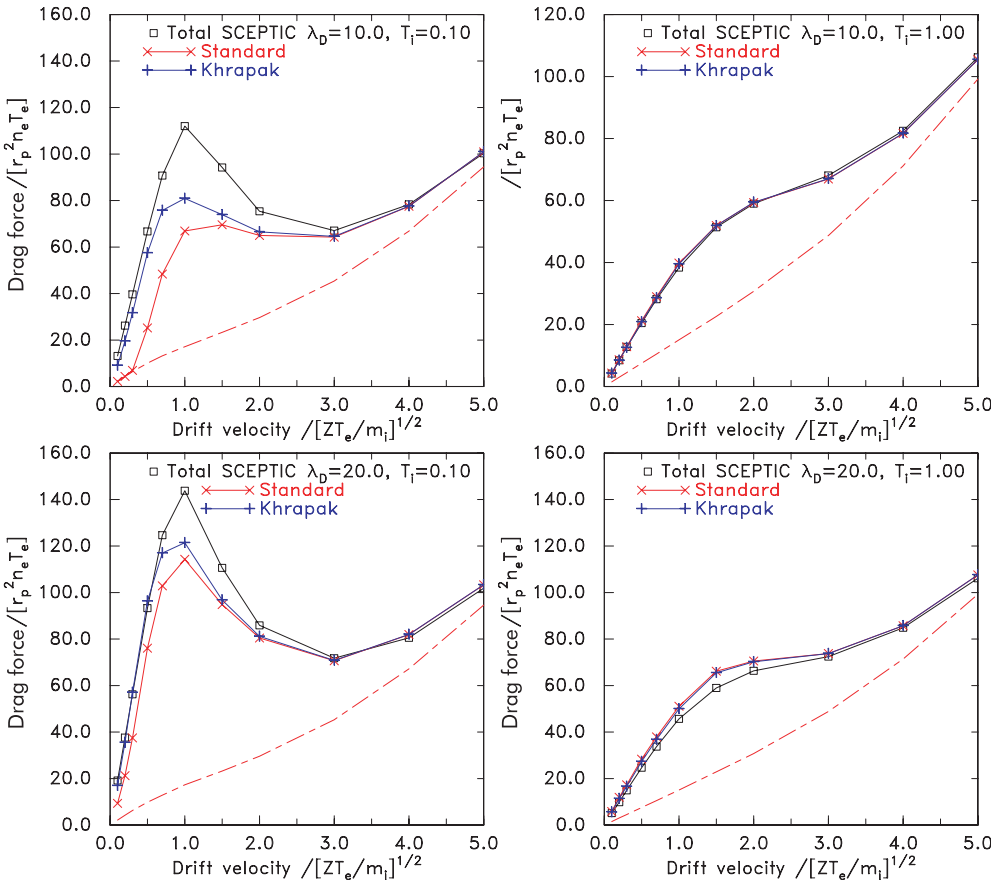

Figure 12. SCEPTIC calculations for $\lambda_{De} = 10$ and 20, on a computational domain of radius 20 and 40 times the probe radius, with $T_i = 0.1$ and 1.0 ZT_e.

obtained with extensions of the Coulomb collision analytic approximations. However the popular approximations give values up to ∼20% different (and even greater at low λ_{De}), even in cases where their assumption of the Debye–Hückel potential form introduces negligible error.

All the results reported here omit effects that might be important in specific experimental or practical situations, notably the effects of collisions, of secondary emission, of possible external plasma non-uniformities and, in the case of dust, of other nearby dust particles. However, this work provides convincing quantitative analysis of the simplified problem of an isolated sphere in an externally uniform collisionless, unmagnetized, flowing plasma, accounting fully for anisotropy and nonlinearity. This hitherto unavailable analysis provides a foundation from which to explore the importance of the other effects.

Acknowledgments

The SCEPTIC calculations were performed on the Alcator Beowulf cluster, which is supported by US DOE grant DE-FC02-99ER54512. I am grateful to S Khrapak for a careful reading of the MS and for drawing reference [32] to my attention.

References

[1] Hutchinson I H 2002 *Plasma Phys. Control. Fusion* **44** 1953
[2] Hutchinson I H 2003 *Plasma Phys. Control. Fusion* **45** 1477
[3] Liboff R L 1959 *Phys. Fluids* **2** 240
[4] Kihara T 1959 *J. Phys. Soc. Japan* **14** 402
[5] Mason E A, Munn R J and Smith F J 1967 *Phys. Fluids* **10** 1827
[6] Hahn H-S, Mason E A and Smith F J 1971 *Phys. Fluids* **14** 278
[7] Al'pert Ya L, Gurevich A V and Pitaevskii L P 1965 *Space Physics with Artificial Satellites* (New York: Consultants Bureau)
[8] Daugherty J E, Porteous R K, Kilgore M D and Graves D B 1992 *J. Appl. Phys.* **72** 3934
[9] Bernstein I B and Rabinowitz I 1959 *Phys. Fluids* **2** 112
[10] Laframboise J G 1966 Theory of spherical and cylindrical Langmuir probes in a collisionless Maxwellian plasma at rest *Technical Report* 100, University of Toronto Institute for Aerospace Studies
[11] Kilgore M D, Daugherty J E, Porteous R K and Graves D B 1993 *J. Appl. Phys.* **11** 7195
[12] Choi S J and Kushner M J 1994 *IEEE Trans. Plasma Sci.* **22** 138
[13] Khrapak S A, Ivlev A V, Morfill G E and Thomas H M 2002 *Phys. Rev.* E **66** 046414
[14] Mott-Smith H M and Langmuir I 1926 *Phys. Rev.* **28** 727
[15] Hutchinson I H 2002 *Principles of Plasma Diagnostics* 2nd ed (Cambridge: Cambridge University Press)
[16] Whipple E C 1981 *Rep. Prog. Phys.* **44** 1197
[17] Lapenta G 1999 *Phys. Plasmas* **6** 1442
[18] Kennedy R V and Allen J E 2001 *J. Plasma Phys.* **67** 243
[19] Allen J E, Boyd R L F and Reynolds P 1957 *Proc. Phys. Soc.* B **70** 297
[20] Bryant P 2003 *J. Phys. D: Appl. Phys.* **36** 2859
[21] Chandrasekhar S 1943 *Astrophys. J.* **97** 255
[22] Cohen R S, Spitzer L and Routly P M 1950 *Phys. Rev.* **80** 230
[23] Barnes M S, Keller J H, Forster J C, O'Neill J A and Coultas D K 1992 *Phys. Rev. Lett.* **68** 313
[24] Nitter T 1996 *Plasma Sources Sci. Technol.* **5** 93
[25] Shukla P K and Mamun A A 2002 *Introduction to Dusty Plasma Physics* (Bristol: Institute of Physics Publishing)
[26] Spitzer L 1962 *Phyics of Fully Ionized Gases* 2nd edn (New York: Interscience)
[27] Draine B T and Salpeter E E 1979 *Astrophys. J.* **231** 77
[28] Khrapak S A, Ivlev A V, Morfill G E, Zhdanov S K and Thomas H M 2004 *IEEE Trans. Plasma Sci.* **32** 555
[29] Hutchinson I H 2004 Potential and frictional drag on a floating sphere in a flowing plasma *Proc. 31st Eur. Conf. on Plasma Physics (London)* (European Physical Society) http://130.246.71.128/pdf/P4_071.pdf
[30] Morfill G E *et al* 1980 *Planet. Space Sci.* **28** 1087
[31] Northrop T G 1992 *Phys. Scr.* **45** 475
[32] Uglov A A and Gnedovets A G 1991 *Plasma Chem. Plasma Process.* **11** 251